

Impact of body position on imaging ballistocardiographic signals

Alexander Woyczyk, Sebastian Zaunseder

Angaben zur Veröffentlichung / Publication details:

Woyczyk, Alexander, and Sebastian Zaunseder. 2023. "Impact of body position on imaging ballistocardiographic signals." In *Proceedings of the 16th International Joint Conference on Biomedical Engineering Systems and Technologies (BIOSTEC 2023), February 16-18, 2023, Lisbon, Portugal - Volume 4: BIOSIGNALS*, edited by Ioanna Chouvarda, Ana Fred, and Hugo Gamboa, 55–65. Setúbal: SciTePress. <https://doi.org/10.5220/0011659900003414>.

Impact of Body Position on Imaging Ballistocardiographic Signals

Alexander Woyczyk¹^a and Sebastian Zaunseder^{1,2} ^b

¹*Faculty of Information Technology, University of Applied Sciences and Arts Dortmund, Dortmund, Germany*

²*Professorship for Diagnostic Sensing, Faculty of Applied Computer Science, University Augsburg, Augsburg, Germany*

Keywords: Imaging Ballistocardiography, Camera Based Monitoring, Physiological Signal Sensing, Heart Rate.

Abstract: Current works direct at the unobtrusive acquisition of vital parameters from videos. The most common approach exploits subtle color variations. The analysis of cardiovascular induced motion from videos (imaging ballistocardiography, iBCG) is another approach that can supplement the analysis of color changes. The presented study systematically investigates the impact of body position (supine vs. upright) on iBCG. Our research directs at heart rate estimation by iBCG and on the possibility to analyse ballistocardiographic waveforms from iBCG. We use own data from 30 healthy volunteers, who went through repeated orthostatic maneuvers on a tilt table. Processing is done according to common procedures for iBCG processing including feature tracking, dimensionality reduction and bandpass filtering. Our results indicate that heart rate estimation works well in supine position (root mean square error of heart rate estimation 5.68 beats per minute). The performance drastically degrades in upright (standing) position (root mean square error of heart rate estimation 21.20 beats per minute). With respect to analysis of beat waveforms, we found large intra-subject and inter-subject variations. Only in few cases, the resulting waveform closely resembles the ideal ballistocardiographic waveform. Our investigation indicates that the actual position has a large effect on iBCG and should be considered in algorithmic developments and testing.


1 INTRODUCTION


Within the last decade, the processing of videos for non-contact acquisition of vital parameters has developed into a large field of research. Particularly for cardiovascular and respiratory monitoring, the technique offers far-reaching opportunities (Molinaro et al., 2022; Zaunseder et al., 2018; Zaunseder and Rasche, 2022). Researchers were able to acquire respiration (van Gastel et al., 2016), oxygen saturation (Moço and Verkruysse, 2021), blood pressure (BP) (Steinman et al., 2021) and local perfusion dynamics (Rasche et al., 2020) from videos. The vast majority of available works directs at the estimation of heart rate (HR) or heart rate variability (HRV), respectively. The most common approach to derive HR or HRV exploits subtle variations in the pixels' intensity. Such variations reflect the varying light absorption due to filling of superficial blood vessels. The similarity to the clinical photoplethysmography (PPG) led to the name imaging photoplethysmography (iPPG).

Instead of exploiting intensity variations, Balakrishnan et al. have shown that HR can be determined by tracking the location of feature points, i.e. not using intensity changes but exploit macro motion (Balakrishnan et al., 2013). The technique closely relates to the well known ballistocardiography (BCG) but uses cameras (in reference to iPPG, we will name it imaging ballistocardiography (iBCG) from here on). Besides information on HR, BCG, particularly the shape of the signal, carries information on other cardiovascular quantities as cardiac output or ventricular ejection time, rendering the technique very interesting for cardiovascular monitoring (Inan et al., 2015; Sadek, 2018). With respect to iBCG, few attention was spent on a deeper characterization including the factors influencing iBCG signals and on the possibilities of using iBCG beyond HR.

Our work aims at a deeper characterization of iBCG. Such investigation is important towards a potential extended usage of iBCG, let it be alone or in combination with iPPG. This paper presents preliminary investigations on the general usability of iBCG for HR and morphological analyses using iBCG in dependency of the body position.

The remainder of the work is structured as fol-

^a <https://orcid.org/0000-0001-6026-8816>

^b <https://orcid.org/0000-0001-6114-3142>

lows. First, we provide the background on BCG in general and present processing approaches for iBCG in particular. In section 3 we detail the pursued processing method and evaluation metrics. In section 4 we present results on the HR estimation by iBCG and analyse the resulting iBCG morphologies. Finally, section 5 discusses our findings and relates them to the literature.

2 BACKGROUND ON BALLISTOCARDIOGRAPHY

2.1 Physiological Background

BCG describes minor movements of the body caused by the blood ejection of the heart. It is closely connected to central haemodynamics, as it measures the effect of the force accelerating the blood from the heart into the aorta and the subsequent directional changes of the blood flow. The terminology of the ballistocardiographic waves was introduced by Starr et al. and describe the body displacement along the longitudinal, i.e. head-to-toe axis (Starr, 1958).

Among several small displacements, a healthy BCG features a prominent movement complex (Figure 1, points I, J and K), which can be directly associated with the ejection of blood from the heart and the following redirection of the blood's movement as it passes the aortic arch. The I-wave is the effect of the force opposing the head-ward acceleration of the blood being ejected from the left ventricle into the aorta. Soon, the main portion of the blood gets redirected and therefore accelerated in foot-ward direction by passing through the aortic arch and entering the abdominal aorta. The deceleration of the head-ward and redirection to toe-ward movement causes the J-wave. Lastly the K-wave is supposed to originate from the deceleration of the blood stream through the descending aorta. (Pinheiro et al., 2010)

Since the BCG directly originates from the blood ejection, the acceleration and redirection of blood flow, it is of high interest to cardiovascular monitoring. The BCG can be used to evaluate various physiological and cardiac parameters, e.g. cardiac output or BP (Javaid et al., 2016; Su et al., 2019). Because of its periodicity with each heart beat it is possible to measure HR and HRV. Since the BCG waves can be linked to different stages of the cardiovascular cycle, the analysis of the signals' shape can yield further information, e.g. it can serve as an indicator of heart disease or stenosis within the aorta (Pinheiro et al., 2010). In combination with other physiological signals as PPG, the BCG can be used to determine pulse

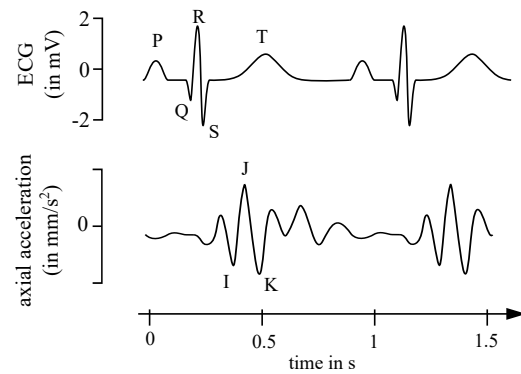


Figure 1: Illustration of the acceleration BCG (axial acceleration) signal together with the ECG. The BCG waveform was modified from Pinheiro et al. (Pinheiro et al., 2010).

transit time (PTT). Examining the PTT can lead to insight on vascular stiffness and is also connected to BP (Leitão et al., 2018; Pielmus et al., 2021).

2.2 Conventional Hardware for Ballistocardiography

Since early descriptions in the 1940s, there have been different approaches to record BCG signals. The most common setup is described by Starr and measures the BCG along the longitudinal axis of the body. This is done either standing on modified scales (Inan et al., 2009) or sitting on a chair with piezoelectric sensors (Alametsä et al., 2004). Another common setup involves the subjects to lay in weight-sensitive beds. As the force is recorded along the sagittal axis (Soames and Atha, 1982), the setup results in a different BCG morphology. Today, the possibilities of small scale acceleration sensors and gyroscopes present in fitness trackers and smart watches allows to measure BCG under various circumstances (Zhang et al., 2021; Shin et al., 2022). The usage of videos is yet another possibility to carry out BCG, which has gained importance in recent years.

2.3 Imaging Ballistocardiography

A fundamental work on BCG measurement from video sequences was presented by Balakrishnan et al. (Balakrishnan et al., 2013). The core idea is to use prominent features in the face area to estimate axial displacement caused by the ejection of blood from the heart. Prominent features are typically pixels with high image gradient as corners or edges and are identified in the first frame. By using the Kanade-Lucas-Tomasi (KLT) algorithm each feature's new location can be retrieved in the consecutive frames (Tomasi and Kanade, 1991). The vertical motion trajectories

of several feature points are then used as input sources for principal component analysis (PCA). In order to determine the heart rate, Balakrishnan et al. select the component with the highest periodicity among the decomposed signals (Balakrishnan et al., 2013).

Shao et al. use a similar set-up, capturing the face with a camera (Shao et al., 2017). Instead of automatically searching for feature points, they manually label prominent characteristics as moles, hair or skin pigmentation and identify corner features using "Good features to track" (Jianbo Shi and Tomasi, 1994). Those features are tracked using KLT and the vertical trajectories are averaged over all features.

Hassan et al. also use KLT to track points within the face (Hassan et al., 2017). Their selection of face features consists of 32 points, horizontally aligned on the forehead and another set of 16 feature points vertically aligned on the nose ridge. The initial positions are determined by using coordinates relative to a face bounding box originating from the Viola-Jones face detector (Viola and Jones, 2001). Using PCA they deconstruct the multivariate signal into its main components and evaluate the distribution of the main frequency of each component in order to estimate the HR.

Li et al. instead mount the camera onto the head of their subjects (Li et al., 2020). Being able to use the whole field of view (FOV) there is a higher probability of detecting high-quality corner features for tracking. Similar to Balakrishnan et al. (Balakrishnan et al., 2013) they use the KLT tracking algorithm to determine movement of the head by the displacement of prominent features in the subjects FOV. Using PCA and frequency analysis they estimate the heart rate as the frequency with the largest amplitude within the range of 0.75 to 3 Hz.

Lee et al. (Lee et al., 2021) present a fusion approach of iPPG and iBCG to estimate HR. They use a deep learning approach, i.e. single shot detector with ResNet, to detect the face and track 80 points in a reduced facial area using the KLT tracker. As before, the iBCG is then extracted using PCA. Finally, Lee et al. combine iBCG information with iPPG to yield a stable HR.

Taken together, the existing approaches except Li et al. (Li et al., 2020) are closely related. Minor differences regarding the area to be considered should not have a strong impact as commonly facial features, excluding the eyes, are used. The feature points itself are typically defined automatically according to the detection of edges in the image. The further processing is always based on the axial displacement. Differences exist regarding additional processing steps, particularly the usage of PCA or not.

Lastly the presented works differ in their approaches on estimating the HR from the calculated iBCG signal, e.g. using the PCA-component with the clearest main frequency (Balakrishnan et al., 2013), peak frequency of the Fourier-transformed signal (Shao et al., 2017; Li et al., 2020; Lee et al., 2021) or the mean of a normal distribution fitted to a set of observed peak frequencies (Hassan et al., 2017).

3 MATERIAL AND METHODS

3.1 Dataset

Overview: The used data originates from own multimodal experiments invoking healthy subjects. Throughout the experiment, each participant executed one or two cold stress tests, went through repeated epochs of paced breathing and repeated orthostatic maneuvers. During the experiment we recorded multiple vital signs and three RGB videos. All subjects gave written consent. The study was approved by the Ethics Committee at TU Dresden (EK 311082018).

Procedure: The subjects were asked to lay down on a tilt-table, where they were connected to the measurement systems. Over a duration of approximately 49 minutes the tilt-table was alternated between supine and upright position every 7 minutes to provoke a cardiovascular reaction. The position change took approximately 10 seconds and was executed with the subject on the table. Each orthostatic maneuver marks the beginning of a new epoch (supine or upright), resulting in a total of seven epochs for each subject. Between orthostatic maneuvers, i.e. within each 7 minute epoch, participants had resting phases and executed at least one cold stress test or paced breathing sequence. During the cold stress test subjects had to submerge their left hand into a basin of cold water ($1 - 4^{\circ}\text{C}$) for a duration of 60 seconds. The paced breathing exercise consisted of following a rhythm of 8 breath cycles per minute for 60 seconds.

Measurements: During the experiment, we recorded RGB videos and multiple vital signs. Videos were recorded with three RGB cameras (UI-3060CP-C-HR Rev 2 by IDS Imaging Development Systems GmbH; Obersulm, Germany). All cameras were fixed on a robust frame joint with the tilt-table and therefore static in their relative position to the subject even during tilting, as can be seen in figure 2. For this work, only Camera 2 is of particular interest. This camera recorded the subject's head at a distance of approximately 40 cm. The recorded area covered the head and a small portion of the shoulders. Videos were captured at a color depth of 12 bit, a frame rate of

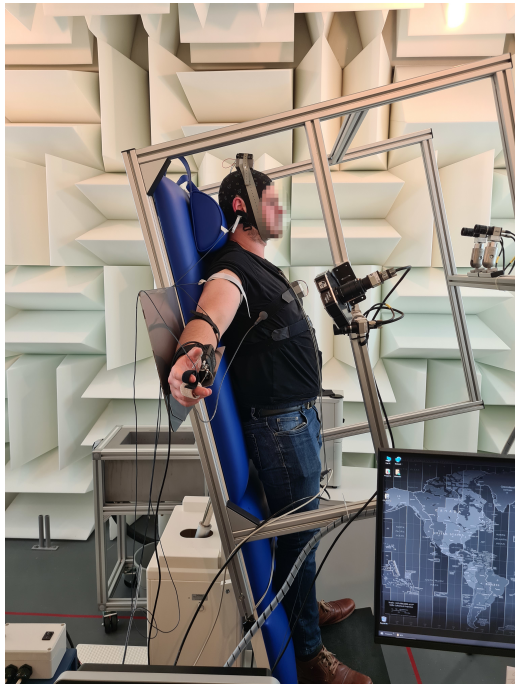


Figure 2: Experiment setup: Subject on tilt table in upright position. Three cameras were attached to the table's frame, additionally ECG, PPG, respiration and BP were recorded.

25 Hz and a spatial resolution of $1280 \text{ px} \times 960 \text{ px}$. The videos were saved in a proprietary format with lossless compression. The recordings took place in a controlled environment using indirect artificial illumination (Walimex pro LED Sirius 160 Daylight 65W by WALSER GmbH & Co. KG; Gersthofen, Germany).

Several physiological signals were recorded to serve as reference, namely PPG and respiration (MP36 by Biopac; Goleta, United States of America) as well as electrocardiography (ECG) and BP monitoring system (Finapres Nova by Finapres Medical Systems; Enschede, Netherlands). The signals of particular relevance for this study were the electrocardiogram (Einthoven II) and a finger PPG signal. We used the PPG signal to assess HR estimation based on iBCG. We used the ECG signal, particularly the time instants of QRS complexes, in order to analyse the waveform from iBCG. Details regarding the handling of reference signals are given in section 3.3.

Used Data: Overall, we use data of 30 healthy subjects (11 female, 19 male; age 20 – 59). From each subject we use excerpts from six epochs, three epochs in supine and three epochs in upright position. Each excerpt has a length of two minutes. During that time, subjects were at rest and quiet. There were no further behavioural advises, still the facial expressions might vary but we would not expect marked movements.

3.2 Video Processing

As stated before, most works on iBCG share a common methodology, i.e. using image features within the face and processing their longitudinal displacement. Following, we present our applied methodology, which closely relates to the core procedure and processing steps of Balakrishnan et al. We also tested some modifications but we will only briefly discuss them in section 5.

3.2.1 Tracking Procedure

As first step to capture head movements, we detect facial landmarks. We use the Viola-Jones face detection to get a estimate of the faces position and size (Viola and Jones, 2001). Landmarks are then identified within the face bounding box and are used to further refine the region of interest (ROI) in which tracking points are located. There are 68 landmarks covering the jaw line, eyes, nose and mouth features. The landmark detection in use is DLib's HOG based implementation of Kazem's "Ensemble of Regression Trees" (Kazemi and Sullivan, 2014; Dlib C++ Library, 2020). Instead of searching the whole face for landmarks, we define a ROI covering an area between mouth and eyes, i.e. we use landmarks at the inner eye corners, mouth and nose. Within this ROI we detect up to 60 feature points using the "Good features to track" algorithm (Jianbo Shi and Tomasi, 1994). The landmarks and feature points are identified in the first frame of each epoch's video segment. In the consecutive frames we use the KLT tracking algorithm to calculate the displacement of each feature points (Tomasi and Kanade, 1991). Figure 3 illustrates the face bounding box, landmark-based ROI and selected feature points by an example.

3.2.2 iBCG Generation

The iBCG signal is generated by evaluating the trajectories of the recorded feature points. As commonly done throughout the literature, we used only the longitudinal axis, i.e. y-component, of each feature point for signal generation. The further iBCG formation follows the ideas of Balakrishnan et al. (Balakrishnan et al., 2013). We discard feature points with large displacement in between frames as it indicates either an unstable feature or possible movement caused by facial expression. A large displacement is defined as a displacement that is higher than the mode of maximum displacements of each feature. This processing step is supposed to eliminate features which can pollute the signal with high displacement values and therefore decrease signal quality. The remaining tra-

jectories are filtered to reduce signal components unrelated to the heart's beating activity. We use a band-pass filter with cutoff frequencies at 0.75 and 5 Hz to cover the signal and its first harmonics, which have an influence on the signal's morphology. The resulting signals serve as input for PCA. PCA decomposes the input signals into its main components, i.e. components responsible for the most variance in the signal. The resulting components are then sorted by their contribution to the signals variance. Finally the most probable candidate component for iBCG is selected by choosing the component with the highest periodicity among the first five components.

3.2.3 iBCG Post Processing

The further processing of iBCG signals differs according to the aim of the analysis, i.e. HR estimation or iBCG morphology analysis.

With respect to HR estimation from iBCG, we introduce an additional bandpass filtering step. As done in comparable works (Balakrishnan et al., 2013; Lee et al., 2021), we employ a fifth-order Butterworth filter with cutoff frequencies at 0.7 Hz and 2.5 Hz. The filtered signal is then transformed to the frequency domain using fast fourier transform (FFT). The FFT is applied to sliding windows of 10 s at a displacement of 1 s. The location of the highest peak between 40 and 180 Hz in the spectrum of each window yields the estimated HR. Due to the overlap of the sliding windows we calculate one HR estimate per second. Each estimate is compared to a reference HR, which is derived from the temporally aligned window applied to the synchronized reference signal (see section 3.3.1 for details).

With respect to beat morphology, as not to impact the waveform, we do not apply additional bandpass filtering.

3.3 Evaluation

3.3.1 Performance of HR Estimation

We use accuracy, root mean square error (RMSE), Bland Altman plots and correlation plots to compare the iBCG approach to a reference HR. The reference HR is derived from the PPG by the following procedure. First, we detect all beats in the PPG excerpt by a customized version of Lázaro et al. (Lázaro et al., 2013). In accordance to the HR estimation by iBCG, we then apply a 10 s sliding window with a step size of 1 s to the detections and derive the reference HR from the median inter-beat distance in each window.

We then calculate the accuracy of our HR estimation from iBCG signals in reference to the PPG HR.

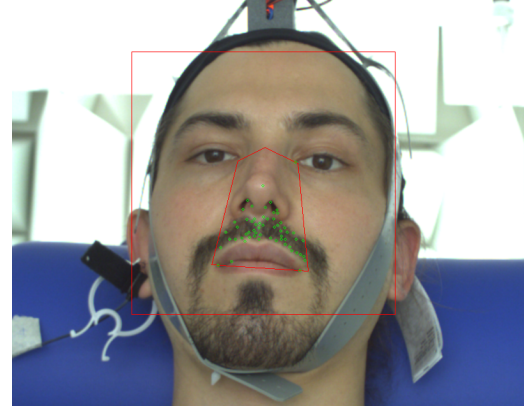


Figure 3: Exemplary illustration of detected feature points, which are subsequently tracked. The image shows the Viola-Jones bounding box (red square), the ROI defined based on selected relevant facial landmarks (inner red polygon) and the feature points (green dots).

The accuracy is defined as the percentage of the estimated HR (further denoted $HR^{(Alg)}$) within 5 bpm of the reference HR (further denoted as $HR^{(Ref)}$).

RMSE is defined by

$$RMSE = \sqrt{\frac{\sum_{n=1}^N \left(HR_n^{(Alg)} - HR_n^{(Ref)} \right)^2}{N}} \quad (1)$$

where n denotes a single window (in our case 10 s).

Though evaluating overlapping windows, we consider each estimate equally as HR estimation was done independently of previously calculated HR estimates. All subjects share the same number of windows for each two-minute excerpt thus yielding equal weight for each subject.

3.3.2 Assessment of Beat Morphology

In accordance to the analysis of BCG signals, our morphology analysis addresses the shape of iBCG beats in the second order derivative, i.e. the acceleration iBCG signal. In order to analyse the shape, we construct beat templates for each epoch by grouping 10 consecutive beats. To delineate single beats, we employ the synchronized reference ECG. We first detect QRS complexes using a customized version of Pan Tompkins QRS detection algorithm (Pan and Tompkins, 1985). Based on the occurrence of QRS complexes, we extract iBCG segments by cutting the signal midway in between QRS complexes. The separated segments are then aligned at the QRS complex' R-peak and a template is generated by averaging the signals of the iBCG segments. We then further improve the template by correcting small phase delays (less than 10 ms) utilizing the cross-correlation between preliminary template and each segment.

The quantitative evaluation of the waveforms directs at the feasibility of morphological analysis of iBCG signals and considers three aspects:

1. Beat-to-beat correlation within groups of 10 consecutive beats: A high beat-to-beat correlation coefficient indicates a stable signal and thus good signal quality including a prominent iBCG wave.
2. Template-to-template correlation within each epoch: High correlation coefficients between templates indicate a reliable signal quality throughout the epoch. This indicator could serve as decision criterion for comparing morphological structures between epochs.
3. Template-to-template correlation between neighbouring epochs: Since epochs alternate between supine and upright position, low correlation coefficients indicate substantial differences in supine and upright BCG morphology.

All correlation coefficients were calculated after accounting for small temporal displacements by using cross-correlation. In addition, for qualitative analyses we consider exemplary waveforms with respect to the expectation on a conventional BCG waveform.

3.4 Comparative Method

We also evaluated vertical displacement trajectories without using PCA, as suggested by Shao et al. (Shao et al., 2017). We used up to 60 feature points, identified by the "Good features to track" algorithm within a reduced face bounding box, i.e. cropped horizontally by 25 % in order to diminish the possibility of background within the ROI. Finally we employ the same bandpass filter (cutoff frequencies 0.75 and 5 Hz) and follow the same post processing steps as described in section 3.2.

4 RESULTS

4.1 Heart Rate Estimation

Figure 4 shows the results of the HR estimation for each epoch. The figure illustrates a pronounced effect of body position. Similarly, Table 1 shows the RMSE for all epochs and supports the observation of notable quality differences between the upright and supine position. More in detail, Figure 5 shows the accuracy per subject and epoch. The graphic illustrates three findings: firstly, as seen before, supine position seems to be highly advantageous regarding accurate HR estimation. Secondly, even on an intra-subject

Table 1: Overall RMSE of estimated HR grouped by body position (all values in bpm).

Method	Position	Epochs		
PCA	supine	5.95	4.94	6.16
	upright	21.78	19.40	22.42
without PCA	supine	19.97	18.86	17.01
	upright	35.49	34.18	37.53

basis the accuracy shows relevant changes between different epochs of the same position. And thirdly, some subjects behave markedly worse in most or all epochs.

4.2 Beat Morphology Analysis

Figure 6 shows the mean inter-beat correlation coefficient of single beats for each epoch and each subject. Evaluating the beat-to-beat correlation coefficient shows a higher value for supine epochs than those in upright position. This indicates a more stable beat morphology in supine position. Creating template beats by grouping several consecutive beats together and then calculating the cross-correlation of templates within one epoch also supports our finding supine position being highly beneficial for iBCG recordings. Figure 7 shows for within-subject comparison mostly a stronger inter-template cross-correlation in supine epochs than in upright position. The high correlation demonstrates that the created templates are similar throughout the whole epoch and therefore suitable candidates for advanced BCG analysis. Also Figure 8 demonstrates a low correlation between templates of neighbouring, i.e. supine vs. upright, epochs. Thus revealing that there are substantial differences in templates from supine and upright recordings.

4.3 Comparative Method

Using the trajectories without further signal decomposition, i.e. PCA, we observed worse HR estimations, as shown in table 1. Also the templates generated with this method are less stable, than the ones produced according to Balakrishnan et al. Even though the results are inferior, it can still be observed, that templates generated from epochs in supine body position tend to be more stable than in upright position.

5 DISCUSSION

Our investigations show that HR estimation by iBCG works well in supine position. Our results are slightly

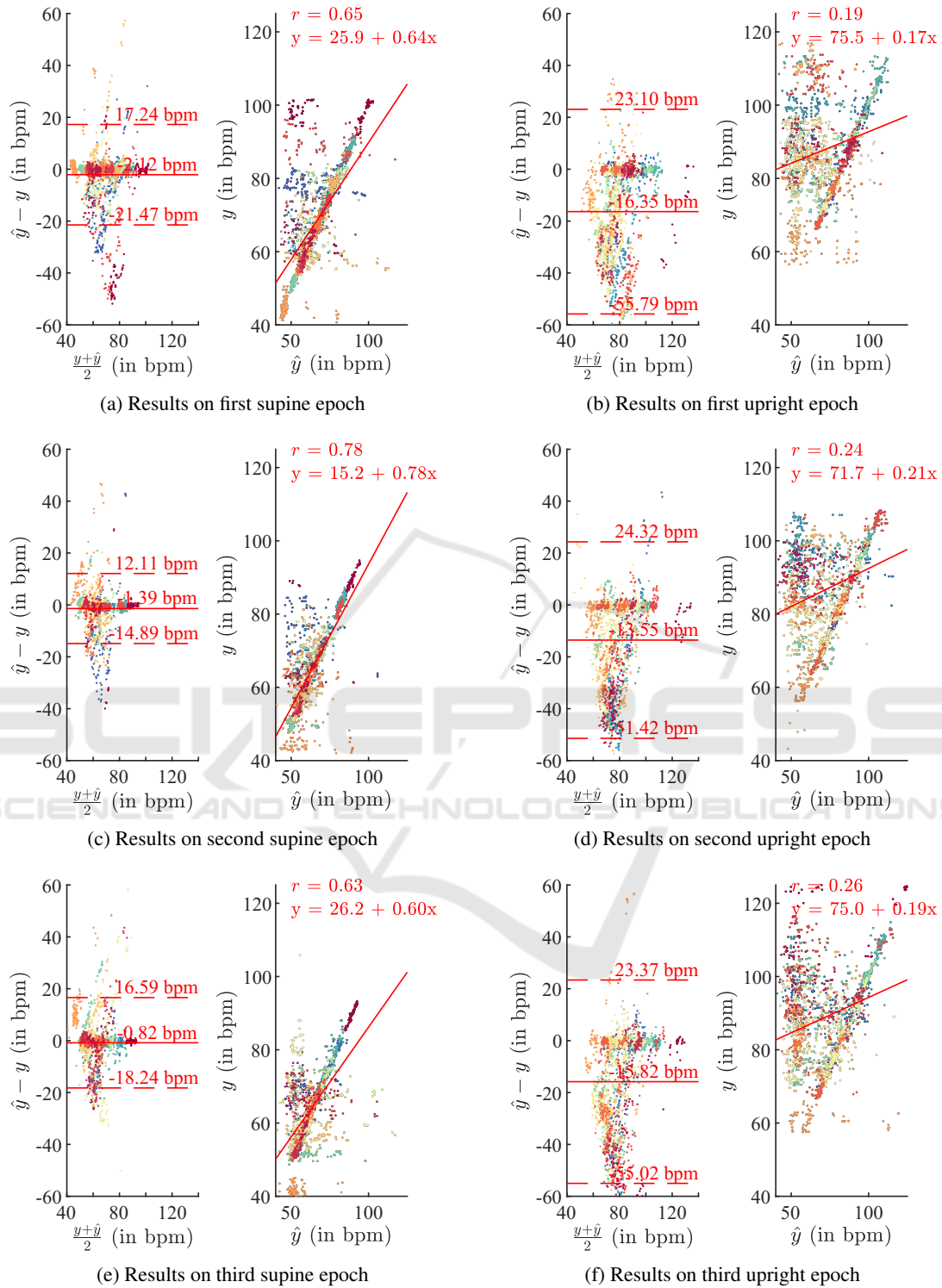


Figure 4: Bland Altman plots and illustration of correlation for all epochs with y as reference HR and \hat{y} as estimated HR. Each point in the plots represents a single 10 s window, each color a subject.

worse than reported in the literature but at an comparable level. E.g. for using iBCG only, Lee et al. report an RMSE of 3.48 bpm, 5.71 bpm and 15.86 bpm for

resting conditions, facial expressions and movements, respectively (correlation coefficients are 0.927, 0.920 and 0.051) (Lee et al., 2021). In general, with re-

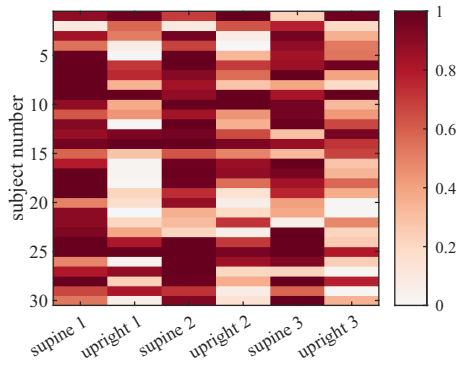


Figure 5: Accuracy matrix showing values for all subjects and epochs. There are distinct differences between supine and upright epochs in almost all subjects.

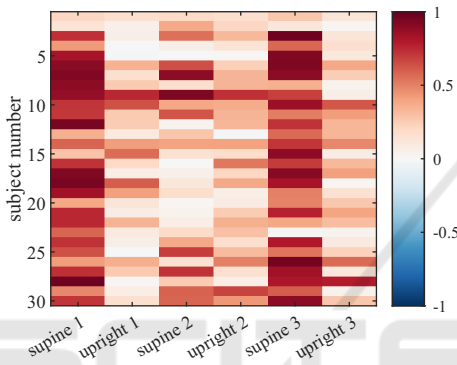


Figure 6: Mean intra-epoch beat correlation on all considered subjects and epochs. The matrix shows the averaged correlation coefficient (after accounting for minor displacement by using cross-correlation) calculated in-between all beats of an epoch.

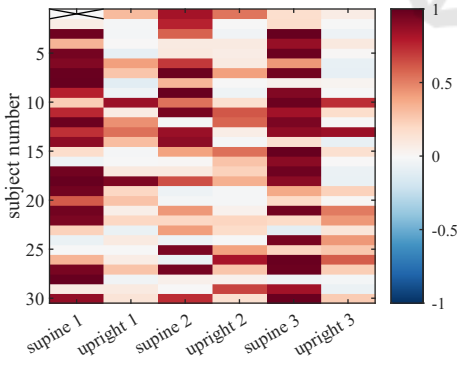


Figure 7: Inter-template correlation of all considered subjects and epochs. The matrix shows the correlation coefficient (after accounting for minor displacement by using cross-correlation) between all templates of an epoch. Due to a delayed start of ECG recording of *Subject 1 - supine 1* only one template could be generated, therefore no correlation was calculated.

spect to the absolute performance of HR estimation, we have to emphasize that our work did not foster an intense optimization, but we adhere to previously

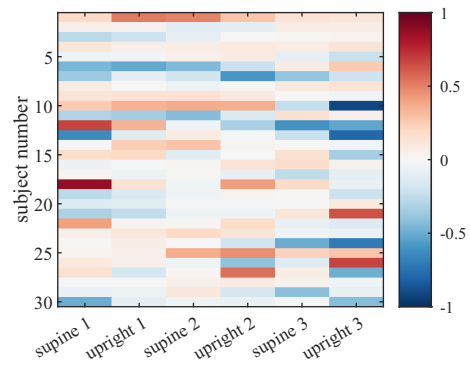


Figure 8: Inter-epoch template correlation between neighbouring epochs. The matrix shows the correlation coefficient (after accounting for minor displacement by using cross-correlation) between all templates of one epoch with all templates of the neighbouring epochs.

published procedures. We thus believe that the results from section 4 could be improved, but this is not our main aim within this work. We consider the found differences between supine and upright position to be of greater importance. The body position obviously has a strong impact on the results as the unsatisfying performance in upright position clearly demonstrates. We did consider other methods and feature points as well, e.g. the method proposed by Shao et al. (Shao et al., 2017). Shao et al. directly exploited axial movements without calculating the acceleration signal. The method thus basically skips some steps of Balakrishnan et al. (Balakrishnan et al., 2013). However, using movements directly, our HR estimation was drastically worse.

With respect to the signal morphology, our findings indicate the iBCG to be troublesome regardless of the body position. While in some cases, as displayed in Figure 10, we could yield a waveform that resembles the well known BCG shape, these cases were the exception rather than the rule. Instead, we often found periodically varying but heavily distorted waveforms and large morphological inter-subject and intra-subject differences, exemplary shown in Figure 9. This observation coincides with exemplary signals from most other works, which do not exhibit distinct BCG characteristics. While a stable waveform and high correlation to the HR make such segments very likely to originate from movement induced by the heart motion, the deformation of the iBCG waveform complicate the analysis of BCG specific features as measuring timings or amplitudes of the BCG complex.

Lastly, we were not able to reproduce the findings of Shao et al., who provide examples of signal shapes that closely match the conventional BCG waveform (Shao et al., 2017). One potential reason

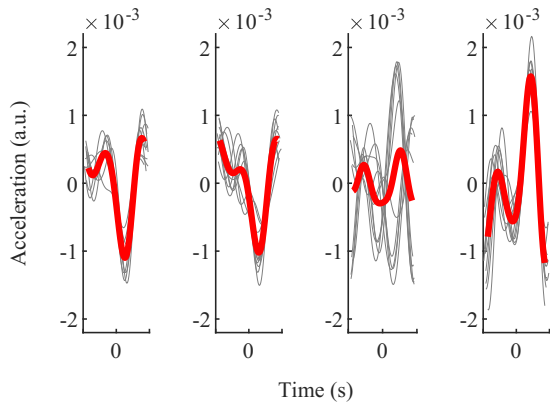


Figure 9: Consecutive templates of varying beats, (subject 11, supine 3). Templates and beats are centered at ECG R-peak.

might be the size of the observed area: if the spatial resolution is too small, detailed ballistocardiographic information might get blurred or lost completely. Another reason could be the careful manual selection of a small ROI with a prominent characteristic as employed by Shao et al. (Shao et al., 2017), which leads to a higher and more distinct waveform.

Concerning posture variations, we did expect differences and some degradation. Jung et al. describe a distinct impact of posture on the BCG morphology (Jung et al., 2020). Similarly, Shin et al. report relevant variation in BCG morphology between standing, sitting and supine positions (Shin et al., 2022). Though both works direct at wrist BCG, facial iBCG signals can be assumed to be affected by positional changes and varying support of the head as well. Against such background, our findings regarding the signals' shape are reasonable, though the (negative) effect is more pronounced than we expected. Again, even with respect to the signals' shape, we would not rule out that methodological developments or different recording parameters, e.g. higher resolution or lower face to camera distance, might improve the results. In fact, as the timing information from iBCG provides highly relevant information, future works should try to enhance and develop methods towards more reliable iBCG waveforms.

6 CONCLUSIONS

Our analyses show that the body position has a relevant impact on the quality of both, heart rate estimation and morphological analysis in iBCG. Such findings are valuable for future research and development, e.g. they indicate that more robust iBCG algorithms should be developed and tested under varying

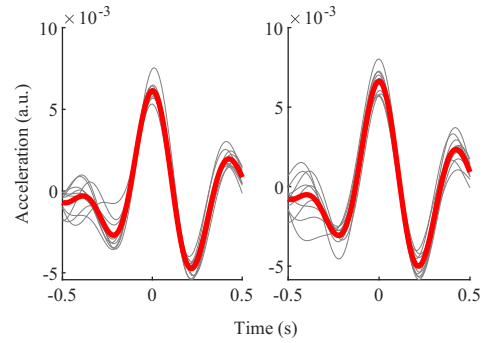


Figure 10: Recognizable BCG morphology (subject 18, supine 1). Templates and beats are centered at ECG R-peak.

positions. As iBCG carries partially redundant and partially complementary information to iPPG, iBCG opens up wide opportunities for sensor data fusion concepts. Particularly the possibility of constructing PPG and BCG signals from the same (camera-)source allows further investigations, as the temporal relationship between heart activity and superficial blood pulsation or the possibility to reduce BCG based artefacts from iPPG. We consider such research and development as very interesting (though challenging) as it has the potential to indirectly improve future applications of iPPG as BP estimation or skin perfusion imaging.

ACKNOWLEDGEMENT

This work was funded by the Deutsche Forschungsgemeinschaft (DFG, German Research Foundation), project 401786308.

REFERENCES

- Alametsä, J., Värri, A., Koivuluoma, M., and Barna, L. (2004). The potential of emfi sensors in heart activity monitoring.
- Balakrishnan, G., Durand, F., and Guttag, J. (2013). Detecting pulse from head motions in video. *Proceedings of the IEEE Computer Society Conference on Computer Vision and Pattern Recognition*, pages 3430–3437.
- Dlib C++ Library (2020). Dlib 19.21 Documentation.
- Hassan, M. A., Malik, A. S., Fofi, D., Saad, N. M., Ali, Y. S., and Meriaudeau, F. (2017). Video-based heart-beat rate measuring method using ballistocardiography. *IEEE Sensors Journal*, 17(14):4544–4557.
- Inan, O. T., Etemadi, M., Wiard, R. M., Giovangrandi, L., and Kovacs, G. T. A. (2009). Robust ballistocardiogram acquisition for home monitoring. *Physiological Measurement*, 30(2):169–185.
- Inan, O. T., Migeotte, P.-F., Park, K.-S., Etemadi, M., Tavakolian, K., Casanella, R., Zanetti, J., Tank, J., Funtova, I., Prisk, G. K., and Di Rienzo, M. (2015).

- Ballistocardiography and Seismocardiography: A Review of Recent Advances. *IEEE Journal of Biomedical and Health Informatics*, 19(4):1414–1427.
- Javaid, A. Q., Ashouri, H., Tridandapani, S., and Inan, O. T. (2016). Elucidating the hemodynamic origin of ballistocardiographic forces: Toward improved monitoring of cardiovascular health at home. *IEEE Journal of Translational Engineering in Health and Medicine*, 4:1–8.
- Jianbo Shi and Tomasi (1994). Good features to track. In *Proceedings of IEEE Conference on Computer Vision and Pattern Recognition CVPR-94*, pages 593–600. IEEE Comput. Soc. Press.
- Jung, H., Kimball, J., Receveur, T., Agdeppa, E., and Inan, O. T. (2020). Quantification of Posture-Induced Changes in Bed-Based Ballistocardiogram. *Computing in Cardiology*, 2020-Sept:2020–2023.
- Kazemi, V. and Sullivan, J. (2014). One millisecond face alignment with an ensemble of regression trees. *Proceedings of the IEEE Computer Society Conference on Computer Vision and Pattern Recognition*, pages 1867–1874.
- Lázaro, J., Gil, E., Vergara, J. M., and Laguna, P. (2013). Pulse rate variability analysis for discrimination of sleep-apnea-related decreases in the amplitude fluctuations of pulse photoplethysmographic signal in children. *IEEE journal of biomedical and health informatics*, 18(1):240–246.
- Lee, H., Cho, A., and Whang, M. (2021). Fusion Method to Estimate Heart Rate from Facial Videos Based on RPPG and RBCG. *Sensors*, 21(20):6764.
- Leitão, F., Moreira, E., Alves, F., Lourenço, M., Azevedo, O., Gaspar, J., and Rocha, L. A. (2018). High-resolution seismocardiogram acquisition and analysis system. *Sensors*, 18(10):3441.
- Li, F., Zhao, Y., Kong, L., Dong, L., Liu, M., Hui, M., and Liu, X. (2020). A camera-based ballistocardiogram heart rate measurement method. *Review of Scientific Instruments*, 91(5).
- Moço, A. and Verkrusse, W. (2021). Pulse oximetry based on photoplethysmography imaging with red and green light. *Journal of Clinical Monitoring and Computing*, 35(1):123–133.
- Molinaro, N., Schena, E., Silvestri, S., Bonotti, F., Aguzzi, D., Viola, E., Buccolini, F., and Massaroni, C. (2022). Contactless Vital Signs Monitoring From Videos Recorded With Digital Cameras: An Overview. *Frontiers in Physiology*, 13:160.
- Pan, J. and Tompkins, W. J. (1985). A real-time qrs detection algorithm. *IEEE transactions on biomedical engineering*, (3):230–236.
- Pielmus, A.-G., Mühlstef, J., Bresch, E., Glos, M., Jungen, C., Mieke, S., Orglmeister, R., Schulze, A., Stender, B., Voigt, V., and Zaunseder, S. (2021). Surrogate based continuous noninvasive blood pressure measurement. *Biomedical Engineering / Biomedizinische Technik*, 66(3):231–245.
- Pinheiro, E., Postolache, O., and Girão, P. (2010). Theory and Developments in an Unobtrusive Cardiovascular System Representation: Ballistocardiography. *The Open Biomedical Engineering Journal*, 4(1):201–216.
- Rasche, S., Huhle, R., Junghans, E., de Abreu, M. G., Ling, Y., Trumpp, A., and Zaunseder, S. (2020). Association of remote imaging photoplethysmography and cutaneous perfusion in volunteers. *Scientific Reports*, 10(1):16464.
- Sadek, I. (2018). Ballistocardiogram Signal Processing: A Literature Review. *arXiv preprint arXiv:1807.00951*.
- Shao, D., Tsow, F., Liu, C., Yang, Y., and Tao, N. (2017). Simultaneous Monitoring of Ballistocardiogram and Photoplethysmogram Using a Camera. *IEEE Transactions on Biomedical Engineering*, 64(5):1003–1010.
- Shin, S., Mousavi, A., Lyle, S., Jang, E., Yousefian, P., Mukkamala, R., Jang, D. G., Kwon, U. K., Kim, Y. H., and Hahn, J. O. (2022). Posture-Dependent Variability in Wrist Ballistocardiogram-Photoplethysmogram Pulse Transit Time: Implication to Cuff-Less Blood Pressure Tracking. *IEEE Transactions on Biomedical Engineering*, 69(1):347–355.
- Soames, R. W. and Atha, J. (1982). Three-dimensional ballistocardiographic responses to changes of posture. *Clinical Physics and Physiological Measurement*, 3(3):169–177.
- Starr, I. (1958). The relation of the ballistocardiogram to cardiac function. *The American Journal of Cardiology*, 2(6):737–747.
- Steinman, J., Barszczyk, A., Sun, H.-S., Lee, K., and Feng, Z.-P. (2021). Smartphones and Video Cameras: Future Methods for Blood Pressure Measurement. *Frontiers in Digital Health*, 3.
- Su, B. Y., Enayati, M., Ho, K. C., Skubic, M., Despins, L., Keller, J., Popescu, M., Guidoboni, G., and Rantz, M. (2019). Monitoring the relative blood pressure using a hydraulic bed sensor system. *IEEE Transactions on Biomedical Engineering*, 66(3):740–748.
- Tomasi, C. and Kanade, T. (1991). Detection and Tracking of Point Features. Technical report, Carnegie Mellon University, Pittsburgh, PA.
- van Gastel, M., Stuijk, S., and de Haan, G. (2016). Robust respiration detection from remote photoplethysmography. *Biomedical Optics Express*, 7(12):4941.
- Viola, P. and Jones, M. (2001). Rapid object detection using a boosted cascade of simple features. In *Proceedings of the 2001 IEEE Computer Society Conference on Computer Vision and Pattern Recognition. CVPR 2001*, volume 1, pages I–511–I–518. IEEE Comput. Soc.
- Zaunseder, S. and Rasche, S. (2022). Chapter 7 - Clinical applications for imaging photoplethysmography. In Wang, W. and Wang, X., editors, *Contactless Vital Signs Monitoring*, pages 149–164. Academic Press.
- Zaunseder, S., Trumpp, A., Wedekind, D., and Malberg, H. (2018). Cardiovascular assessment by imaging photoplethysmography-a review. *Biomedizinische Technik*, 63(5):529–535.
- Zhang, Y., Zhang, X., Cui, P., Li, S., and Tang, J. (2021). Key Feature Selection and Model Analysis for Blood Pressure Estimation from Electrocardiogram, Ballis-

tocardiogram and Photoplethysmogram. *IEEE Access*, 9:54350–54359.

APPENDIX

Accuracy and correlation matrices of the processing steps without PCA as described in section 3.4 are presented below.

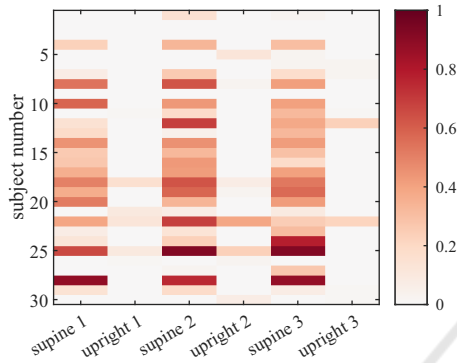


Figure 11: Without PCA processing: Accuracy matrix showing values for all subjects and epochs. There are distinct differences between supine and upright epochs in almost all subjects.

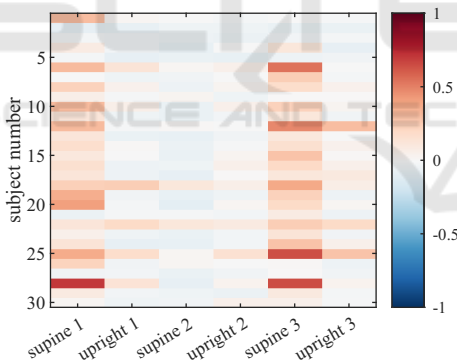


Figure 12: Without PCA processing: Mean intra-epoch beat correlation on all considered subjects and epochs. The matrix shows the averaged correlation coefficient (after accounting for minor displacement by using cross-correlation) calculated in-between all beats of an epoch.

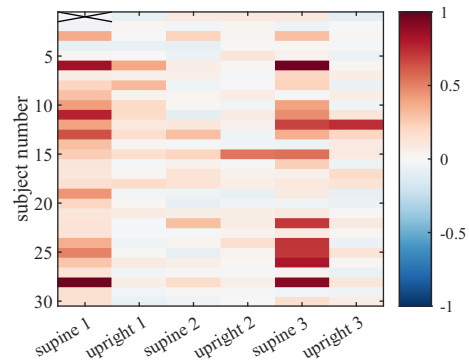


Figure 13: Without PCA processing: Inter-template correlation of all considered subjects and epochs. The matrix shows the correlation coefficient (after accounting for minor displacement by using cross-correlation) between all templates of an epoch.

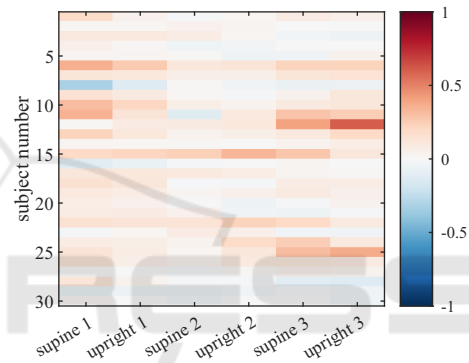


Figure 14: Without PCA processing: Inter-epoch template correlation between neighbouring epochs. The matrix shows the correlation coefficient (after accounting for minor displacement by using cross-correlation) between all templates of one epoch with all templates of the neighbouring epochs.